

# Tensor force and shape evolution of Si isotopes in Skyrme-Hartree-Fock model

A. Li<sup>1,2,3,\*</sup>, X. R. Zhou<sup>4,\*</sup>, and H. Sagawa<sup>1,5,\*</sup>

<sup>1</sup>*RIKEN, Nishina Center, Wako 351-0198, Japan*

<sup>2</sup>*Department of Astronomy and Institute of Theoretical Physics and Astrophysics, Xiamen University, Xiamen 361005, China*

<sup>3</sup>*State Key Laboratory of Theoretical Physics, Institute of Theoretical Physics, Chinese Academy of Sciences, Beijing, 100190*

<sup>4</sup>*Department of Physics and Institute of Theoretical Physics and Astrophysics, Xiamen University, Xiamen 361005, China*

<sup>5</sup>*Center for Mathematics and Physics, University of Aizu, Aizu-Wakamatsu, Fukushima 965-8560, Japan*

\**E-mail: liang@xmu.edu.cn (AL); xrzhou@xmu.edu.cn (XZ); sagawa@u-aizu.ac.jp (HS)*

.....  
 Much interest has been devoted to the shape evolution of neutron-rich Si isotopes recently both experimentally and theoretically. We provide our study of <sup>28–42</sup>Si by Skyrme-Hartree-Fock model with BCS approximation for the pairing channel. We use an empirical pairing parameter deduced from the experimental binding energy data for each nuclei and each Skyrme parametrization. The recent highlight of the deformation change from a prolate shape of <sup>38</sup>Si to an oblate shape of <sup>42</sup>Si is confirmed in the present model. We also emphasize the role of tensor force on deformations of neutron-rich <sup>30,32</sup>Si, and discuss its underlying physics.

## 1. Introduction

The disappearance of  $N = 28$  shell closures has been a huge debate in recent years, especially after the conflicting experimental evidence on the structure of <sup>42</sup>Si coming from MSU [1] and GANIL [2]. The small two-proton removal cross section in the first experiment was interpreted as a doubly closed-shell structure with a large  $Z = 14$  subshell gap at  $N = 28$ , indicating a nearly spherical shape of this nucleus. Contrary to this result, the observation of a very low-lying  $2^+$  state at GANIL supports the vanishing of the  $N = 28$  shell closure and a largely-deformed shape for <sup>42</sup>Si. The later claim actually has been theoretically pointed out in several studies with shell-model and mean-field approaches [3–10]. These studies predict the spherical neutron shell closure is broken already in the mean-field level [3–8], and the shape coexistence is present in some nuclei along the  $N = 28$  isotone, due to a soft energy surface [3, 4]. Some articles have also considered the possible influence of the  $\gamma$ -softness found in the neutron-rich Si region [3, 4, 9].

In Ref. [3], comparisons were made among the Skyrme-Hartree-Fock (SHF) approach, the relativistic mean-field (RMF) model, and the finite-range droplet model (FRDM) for the quadruple deformation of Si isotopes. These models gave consistent ground-state shape predictions for <sup>28</sup>Si ( $N = Z = 14$ ), <sup>34</sup>Si ( $N = 20, Z = 14$ ), and <sup>42</sup>Si ( $N = 28, Z = 14$ ): oblate for <sup>28,42</sup>Si and spherical for <sup>34</sup>Si. The non-magic nature of <sup>42</sup>Si was noted then as an interesting phenomenon. The reason for this is attributed recently to the tensor effect on the change of

---

shell structure in neutron-rich nuclei [9–13]. This tensor interaction acts directly on the  $1d$  spin-orbit splitting, and gives a smaller  $2s_{1/2}$ - $1d_{5/2}$  proton gap when more neutrons occupy  $1f_{7/2}$  orbit. This feature is later analyzed in details by Tarpanov et al. [14] within various mean-field models assuming the spherical symmetry. They have demonstrated that the tensor component in the effective interaction governs the reduction of the  $1d$  proton spin-orbit splitting when going from  $^{34}\text{Si}$  to  $^{42}\text{Si}$ . Also the magnitude of the change is consistent with the empirical observations. It is necessary to extend the study of tensor correlations not only for the spin-orbit splitting but also for the evolution of deformed nuclei as will be done in the present work. In addition, the inclusion of tensor terms in the calculations have achieved considerable success in explaining several nuclear structure problems not only in the ground states [15–17] but also in the excited states [18–20]. In the present study we focus on the tensor effect on the shape evolution of Si isotopes, for example: is the tensor-force-driven deformation present in other neutron-rich Si isotopes, especially  $^{30}\text{Si}$  with a possible  $N = 16$  subshell, since some models (for example, the FRDM [21]) predicted a spherical for this nucleus [3] while the large  $B(E2)$  value suggested its deformed nature [22].

For this purpose, we use the deformed Skyrme-Hartree-Fock model (DSHF) [23] with BCS approximation for the nucleon pairing. As well-known, the standard BCS treatment of pairing was criticized to have the unphysical particle-gas problem [24] when applied to neutron-rich isotopes, namely, there is an unrealistic pairing of highly excited states. To cure this defect to some extent, a smooth energy-dependent cut-off weight was introduced [25, 26] in the evaluation of the local pair density, to confine the region of the influence of the pairing potential to the vicinity of the Fermi surface. Some work also tried a variant calculation with weak pairing [3, 27]. In the present study, the above-mentioned cut-off weight is incorporated in the BCS approximation, and for each nucleus the pairing parameter is obtained with full respect of the empirical data of pairing gaps, extracted by using the experimental binding energies of Ref. [28] and the three-point mass difference formula [29]:  $\Delta^{(3)}(A) = \frac{(-)^A}{2}[B(A) + B(A - 2) - 2B(A - 1)]$  with  $B(A)$  the binding energy of nucleus with even mass number  $A$ . We employ several recent Skyrme parametrizations with various tensor couplings to explore the role of tensor force on the shape of neutron-rich Si isotopes, and theoretical results will be confronted directly with recent experiments.

The paper is organized as follows. In Sec. II, we outline the necessary formalism. The numerical results and discussions are given in Sec. III. Finally, Sec. IV contains the main conclusions of this work.

## 2. Formalism

We use the DSHF method [23] solved in the coordinate space with axially symmetric shape [30]. The pairing correlations are taken into account by the BCS approximation with a density-dependent pairing as done in Ref. [27, 31, 32]. Further details can be found in the above references and are not repeated here.

The tensor force is included in the same manner with in Refs. [15–17, 27, 33], with  $T$  and  $U$  denoting the coupling constants representing the strength of the triplet-even and triplet-odd tensor interaction, respectively. It contributes to the Skyrme energy functional  $H^{\text{Sk}}$  in

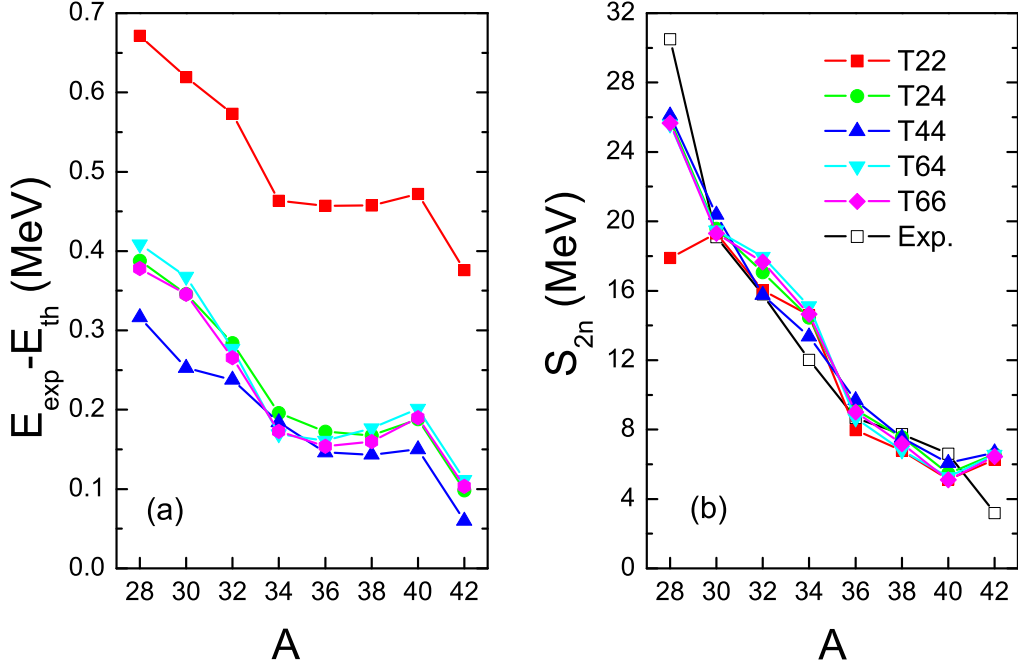


**Fig. 1** (Color online) Left panel: the deviation of the theoretical binding energies from the experimental values [28] for  $^{28-42}\text{Si}$  calculated with effective forces T22, T24, T44, T64, and T66; Right panel: the two-neutron separation energies  $S_{2n}$  in  $^{28-42}\text{Si}$  calculated with effective forces T22, T24, T44, T64, and T66, in comparison with those of the experimental data [28].

a combined way with the exchange term of central part as

$$H_T^{\text{Sk}} = \frac{1}{2}\alpha(J_n^2 + J_p^2) + \beta\vec{J}_n \cdot \vec{J}_p; \quad (1)$$

$$\alpha = \alpha_C + \alpha_T; \quad \beta = \beta_C + \beta_T \quad (2)$$

$$\alpha_C = \frac{1}{8}(t_1 - t_2) - \frac{1}{8}(t_1x_1 + t_2x_2);$$

$$\beta_C = -\frac{1}{8}(t_1x_1 + t_2x_2) \quad (3)$$

$$\alpha_T = \frac{5}{12}U; \quad \beta_T = \frac{5}{24}(T + U). \quad (4)$$

where subscripts  $T$  and  $C$  indicate the tensor and the central contributions, respectively, and  $J_q$  ( $q = n, p$ ) is the spin-orbit density.  $\alpha$  represents the strength of like-particle coupling between neutron-neutron or proton-proton, and  $\beta$  is that of the neutron-proton coupling. With the contributions of tensor interactions, the spin-orbit potential is given by,

$$W_q = \frac{W_0}{2r} \left( 2\frac{d\rho_q}{dr} + \frac{d\rho_{q'}}{dr} \right) + \left( \alpha\frac{J_q}{r} + \beta\frac{J_{q'}}{r} \right). \quad (5)$$

where the first term comes from the Skyrme spin-orbit interaction whereas the second one includes both the central exchange and tensor contributions. The interactions between like (unlike) particles are denoted  $q(q')$  in Eq. (5). Our selected parametrizations are from the recently-built 36 effective interactions with systematically adjusting of the tensor coupling

strengths [17], which include: the Skyrme force T22 serving as a reference with vanishing  $J^2$  terms, T24 with a substantial like-particle coupling constant  $\alpha$  and a vanishing proton-neutron coupling constant  $\beta$ ; T44 with a mixture of like-particle and proton-neutron tensor terms, T62 with a large proton-neutron coupling constant  $\beta$  and a vanishing like-particle coupling constant  $\alpha$ ; and T66 with large and equal proton-neutron and like-particle tensor-term coupling constants. The coupling strengths of various parameter sets used in this study are collected in Tab. 1. To check the capability of the above-selected effective forces with tensor terms, we display in Fig. 1 the deviations of the calculated energies (left panel) from the experimental data, and the predicted two-neutron separation energies (right panel) in comparison with experiments for  $^{28-42}\text{Si}$ . Experimental values are based on Ref. [28]. All the effective interactions overestimate the binding energy (less than 0.7 MeV) along the isotopic chain. However, the interactions with tensor terms (T24, T44, T64, and T66) give better descriptions than the interaction T22 with the absence of tensor terms. This is also true for the case of two-neutron separation energies  $S_{2n}$ . All of T24, T44, T64, and T66 with the tensor terms are reasonably well to describe the energy data  $S_{2n}$ . One should notice that the two-neutron separation energies are not close to zero in Fig. 1, more than 3 MeV even in  $^{42}\text{Si}$ . Thus we can conclude that all the nuclei discussed in the present study are not loosely-bound nuclei, which may justify the usage of BCS treatment for the pairing channel.

**Table 1** Coupling strengths (in MeV) of various parameter sets used in the work.

	T22	T24	T44	T64	T66
$\alpha$	0	120	120	120	240
$\beta$	0	0	120	240	240
$\alpha_T$	-90.6	24.7	8.97	-0.246	113
$\beta_T$	73.9	19.4	113	218	204

The pairing interaction is written as

$$V_{\text{pair}}(\mathbf{r}_1, \mathbf{r}_2) = V_{\text{pair}} \left( 1 - \frac{\rho(\mathbf{r})}{\rho_0} \right) \delta(\mathbf{r}_1 - \mathbf{r}_2). \quad (6)$$

where  $\rho(\mathbf{r})$  is the Hartree-Fock (HF) matter density at  $\mathbf{r} = (\mathbf{r}_1 + \mathbf{r}_2)/2$  and  $\rho_0 = 0.16 \text{ fm}^{-3}$ . The pairing strengths  $V_{\text{pair}}$  for each Skyrme force are determined to reproduce the empirical neutron pairing gaps in the corresponding nuclei. The gap data and the chosen pairing strengths adopted for  $^{28-42}\text{Si}$  are presented in the upper and lower panel of Fig. 2, respectively. As a result the pairing strengths for all the chosen effective forces tend to have an average value around  $900 \sim 1000 \text{ MeV fm}^3$  with variations up to  $200 \text{ MeV fm}^3$ .

### 3. Results

We display in Fig. 3 the energy surfaces of  $^{30}\text{Si}$  (left panel) and  $^{32}\text{Si}$  (right panel) as a function of the quadrupole deformation parameter  $\beta_2$  using T22, T24, T44, T64, and T66. The energy minima are indicated with triangles. To facilitate the comparison, we shift the energy surfaces with T22 by a constant amount as indicated in the figures.  $^{30}\text{Si}$  is suggested to be deformed as mentioned in the introduction, but T22 and T44 with relatively large pairing strengths ( $\sim 1000 \text{ MeV fm}^3$ ) fail to give deformed energy minima. On the contrary, deformed ground

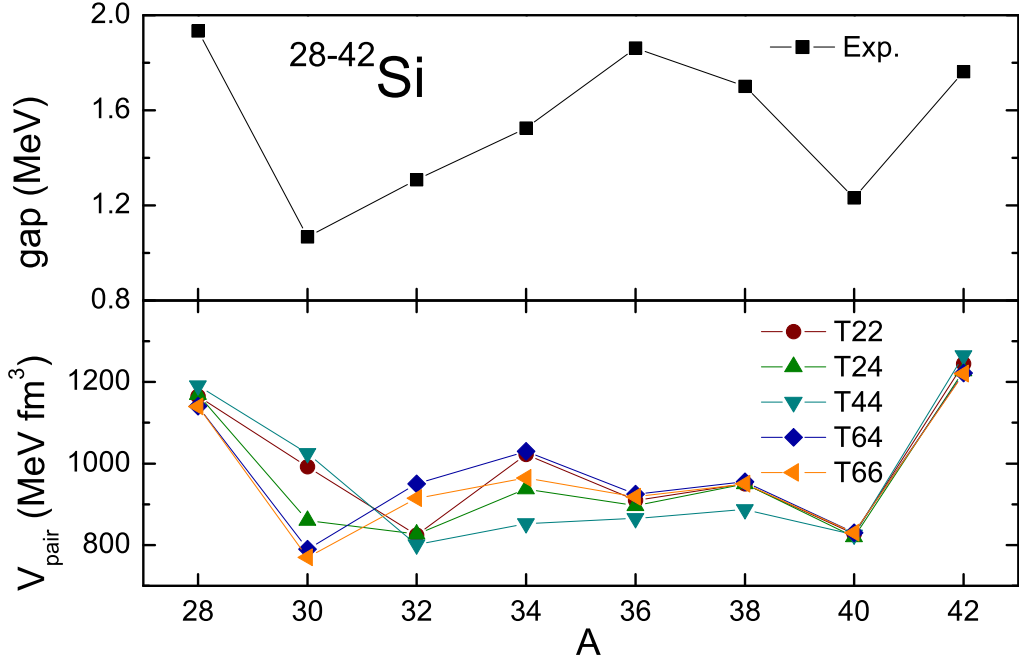


**Fig. 2** (Color online) Upper panel: empirical neutron pairing gaps of Si nuclei  $^{28-42}\text{Si}$ ; Lower panel: adopted pairing strengths  $V_{\text{pair}}$  corresponding to the Skyrme effective force T22, T24, T44, T64, and T66.

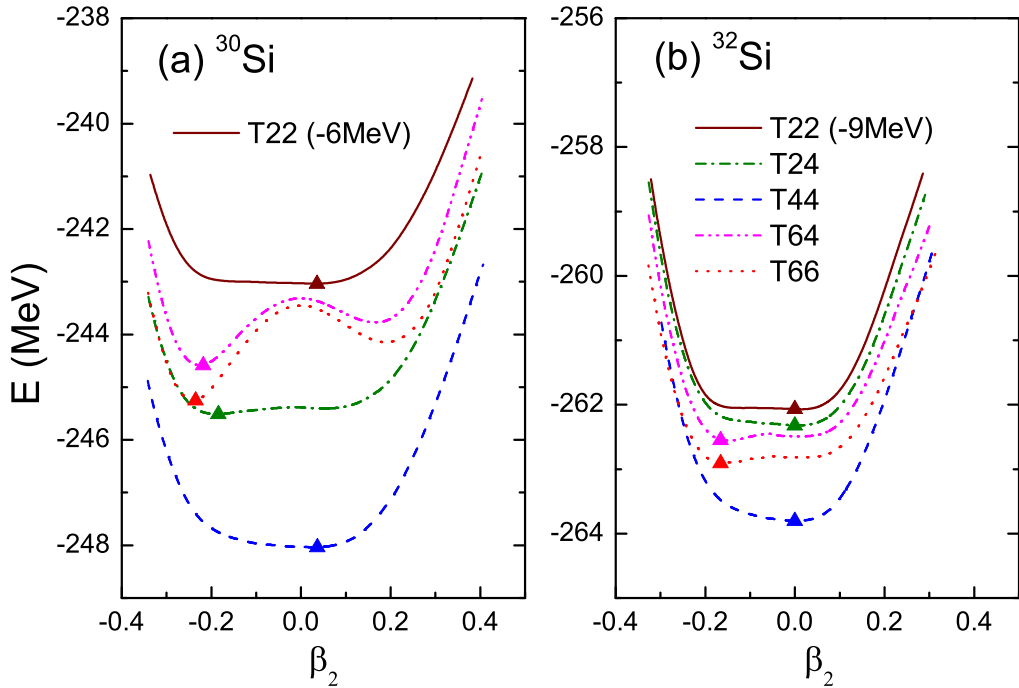


**Fig. 3** (Color online) Energy surfaces of  $^{30}\text{Si}$  (left panel) and  $^{32}\text{Si}$  (right panel) as a function of the quadrupole deformation parameter  $\beta_2$  using T22, T24, T44, T64, and T66. The results with T22 are shifted by  $-6$  MeV and  $-9$  MeV in  $^{30}\text{Si}$  and  $^{32}\text{Si}$ , respectively. The energy minima are indicated with triangles.

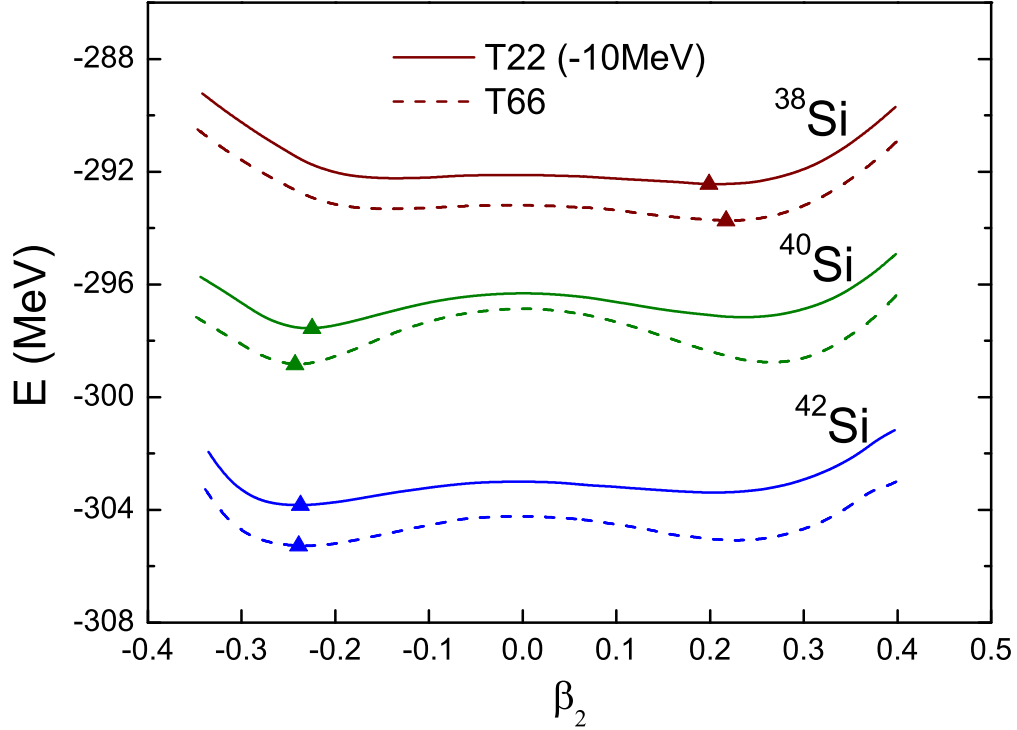


**Fig. 4** (Color online) Energy surfaces of  $^{38-42}\text{Si}$  as a function of the quadrupole deformation parameter  $\beta_2$  using T22 and T66. The results with T22 are shifted by  $-10$  MeV. The energy minima are indicated with triangles.

states can be achieved using the T24, T64 and T66 parametrizations with resulting small pairing strengths ( $\sim 800$  MeV fm $^3$ ). The predicted oblate shape of this nuclei is consistent with the recent RMF result [8]. One should note that the same gap data have been used to deduce the pairing parameters for the different Skyrme interactions, and the variation of pairing parameters is only aimed to reproduce the experimental data. The interesting performance of a weak nucleon pairing may stem from a well-known fact that the pairing interaction forms the  $J = 0^+$  pairs of identical particles which have spherically symmetric wave functions, and as a result, nuclei tend to be more spherical in the cases of T22 and T44 with stronger pairing couplings. This suggests that the resulting shape of a nucleus is sensitive to the nuclear pairing in each nucleus [27], and the experimentally-determined deformed shape of  $^{30}\text{Si}$  favors relatively weak pairing correlations present in the Skyrme effective force T24, T64 and T66. We also notice that large tensor terms present in T64 and T66 tend to make the energy surface deep, namely the tensor force affects dramatically to create a well-deformed ground state for  $^{30}\text{Si}$ . The importance of tensor force will be seen also in  $^{32}\text{Si}$  as shown in the right panel of the same figure. Its shape is predicted to be spherical with T22, T24 and T44, but oblate with T64 and T66 with large tensor terms.

Before proceeding to study in details the tensor role, we prepare in Fig. 4 the energy surfaces of  $^{38-42}\text{Si}$  with two forces T22 and T66, as two representatives to show the common features among the five parameter sets in the present model. It is clearly shown that the oblate shape of  $^{42}\text{Si}$  is quite robust for different tensor couplings, which justifies the broken of  $N = 28$  shell closure seen in a simple single-particle (s. p.) shell-model picture. Also, large

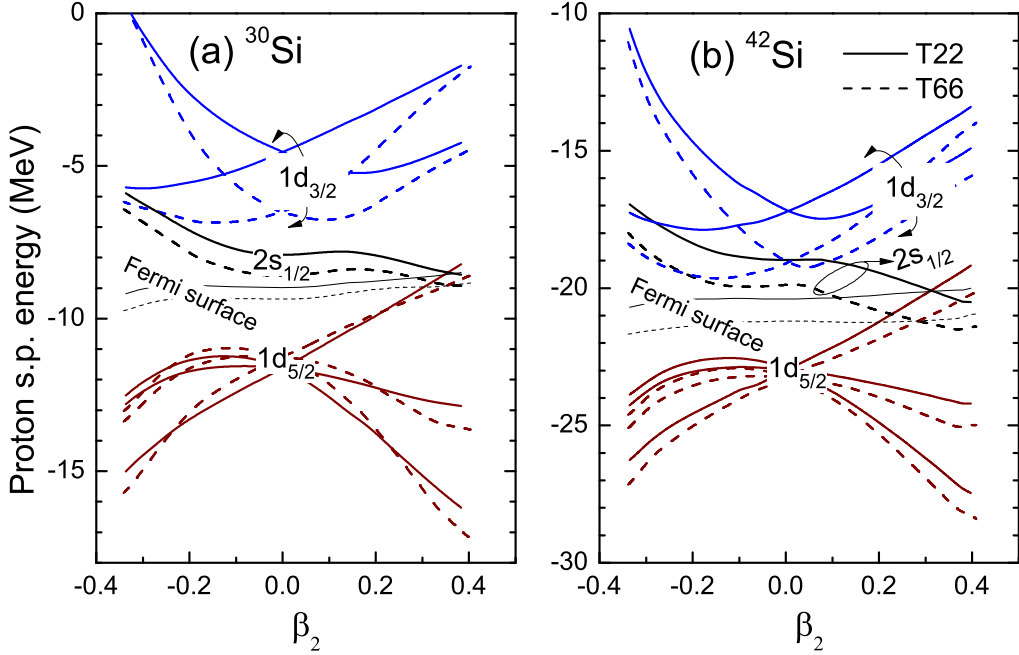


**Fig. 5** (Color online) The s. p. energy levels of protons for  $^{30}\text{Si}$  (left panel) and  $^{42}\text{Si}$  (right panel) are shown as a function of the quadrupole deformation parameter  $\beta_2$  using T22 (solid lines) and T66 (dashed lines). The Fermi surface is also shown between  $2s_{1/2}$  and  $1d_{5/2}$  orbits in the spherical limit.

deformations are expected for  $^{38,40}\text{Si}$  from their measured large  $B(E2)$  values between the  $2_1^+$  and the  $0_1^+$  states [2, 22]. The opposite sign of the deformation parameter  $\beta_2$  for  $^{40}\text{Si}$  was predicted by the RMF model and the FRDM model [3]. Experimentally the sign of deformation will be determined by the measurement of its quadrupole moment, and we do not draw any conclusion about this in the present work. One more interesting feature is the deformation change from  $^{38}\text{Si}$  to  $^{42}\text{Si}$  with the increase of neutron number: the energy minima move from the prolate side in the lighter nucleus  $^{38}\text{Si}$  to the oblate side in the heavier nucleus  $^{42}\text{Si}$ . We should notice that this feature of shape evolution will always appear in the present model, despite the employed Skyrme effective force.

Since the tensor force operates strongly between neutrons and protons, the isotope dependence of tensor correlations could be manifested in the difference of the proton s. p. orbits between  $^{30}\text{Si}$  and  $^{42}\text{Si}$ . We present in Fig. 5 the single proton levels in both  $^{30}\text{Si}$  (left panel) and  $^{42}\text{Si}$  (right panel) as a function of the quadrupole deformation parameter  $\beta_2$  using T22 (solid lines) and T66 (dashed lines). We choose T22 and T66 to compare two extreme cases, i.e., T66 with the largest tensor terms and T22 without the tensor terms. The Fermi surface is also shown between  $2s_{1/2}$  and  $1d_{5/2}$  orbits in the spherical limit. Since  $\alpha$  and  $\beta$  are positive in Eq. (5) for T66 case, the protons and the neutrons in  $1d_{5/2}$  orbit decrease the proton spin-orbit splitting in  $^{30}\text{Si}$  as shown in the left panel of Fig. 5. Two main features can be seen as the tensor effect to compare the results between T22 and T66 for  $^{30}\text{Si}$ : a narrower  $1d_{3/2}$ - $1d_{5/2}$  gap and a steeper  $1d_{5/2}$  orbits downward in the oblate side. Then, in the case of T66, more mixing between  $1d_{3/2}$  and  $1d_{5/2}$  results in an oblate shape for this nuclei in

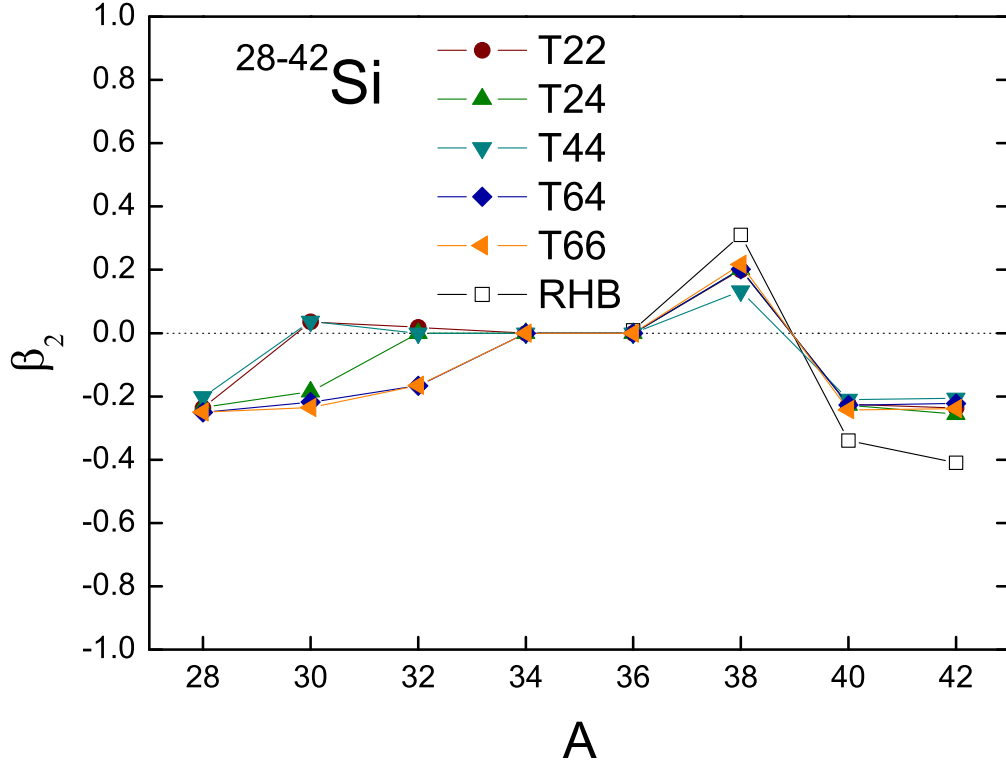


**Fig. 6** (Color online) Deformation parameters  $\beta_2$  as a function of the mass number in comparison with the RHB results [5]. The calculated values corresponding to the Skyrme effective force T22, T24, T44, T64, and T66.

comparison with the case of T22. The shell gap by T66 interaction is narrower also in  $^{42}\text{Si}$  due to the protons in the  $1d_{5/2}$  orbit and the neutrons in  $1f_{7/2}$  orbit as seen in the right panel of Fig. 5. However, both T22 and T66 give oblate deformations, since the tensor effect in this nuclei is not as evident as the case of  $^{30}\text{Si}$  regarding the  $1d_{5/2}$  orbits.

Finally we collect in Fig. 6 the evolution of the quadrupole deformations  $\beta_2$  with mass number  $A$  along the silicon isotopic chain for various effective interactions, in comparison with the Relativistic-Hartree-Bogoliubov (RHB) results [5]. In general, the deformation evolution with increasing neutron number demonstrates clearly the typical Jahn-Teller effect [34]: centered with a spherical shape for  $^{34}\text{Si}$  nucleus at a closed shell, the isotope chain evolves from an oblate shape to a prolate shape. All parametrizations in Fig. 6 predict an oblate shape for  $^{28,40,42}\text{Si}$ , a spherical shape for  $^{34,36}\text{Si}$ , and a prolate shape for  $^{38}\text{Si}$ . The spherical shape of  $^{34}\text{Si}$  is expected because of the neutron closed shell  $N = 20$ . The same spherical shape might be also expected in  $^{36}\text{Si}$  because two neutrons outside of the  $N = 20$  closed shell is not enough to make a deformation. However, the tensor force has a large effect in nuclei  $^{30,32}\text{Si}$  deepening the energy surfaces at oblate energy minima in these nuclei. This mechanism can be understood from the shell gap narrowing due to the tensor force showing in the left panel of Fig. 5.



---

## 4. Conclusion

In summary, we have applied the DSHF model to study the tensor effect on the evolution of the quadruple deformation in Si isotopes, using the experimentally-determined pairing strengths. We found a manifestation of tensor correlations in several isotopic nuclei, such as  $^{30,32}\text{Si}$ , in competition with the pairing correlations. Generally, the tensor force helps to achieve a well-deformed local minimum, by reducing the shell gaps and enhancing s. p. level densities near the Fermi level. In our calculations, the effect of tensor force emerges evidently when we compare the calculated shapes of  $^{32}\text{Si}$  with increasing tensor terms in the employed HF energy density. Large tensor correlations result in a larger deformation for this nuclei, in comparison with a spherical result with small tensor forces. The tensor-force-driven deformation in this nuclei is something we should pay much attention to, since it relates to a further improvement of many theoretical models or parametrizations, such as shell model and the SHF model, toward a better description for the shell structures of nuclei in general. On the other hand, the pairing interaction among nucleons is introduced in this work using the BCS treatment. We take the strength parameters fully consistent with the empirical gap data. For the chosen various Skyrme parametrizations, we find that the resulting pairing strengths are not so much varied around the average value around  $V_{\text{pair}} = 900 \sim 1000 \text{ MeV fm}^3$ . However, the resulting nuclear shapes are sensitive to the adapted pairing strengths. That is, to take  $^{30}\text{Si}$  as an example, T22 and T44 with the larger values around  $1000 \text{ MeV fm}^3$ , give no deformation, while T24, T64, and T66 with the smaller values around  $800 \text{ MeV fm}^3$  give a large oblate deformation. We notice that the latter case is preferred by the recent experiments. This means the Skyrme interactions T24, T64, T66 give a better description of  $^{30}\text{Si}$ . Finally, all the listed effective forces in this work show a prolate-to-oblate transition with increasing number of neutrons from  $^{38}\text{Si}$  to  $^{42}\text{Si}$  as a typical Jahn-Teller effect. To further disentangle the prolate or oblate nature of  $^{40}\text{Si}$ , the Coulomb excitation could be the best experimental tool to find out the sign and the magnitude of the quadrupole deformation. The measurements of quadruple moments of its neighboring nuclei (such as  $^{39}\text{Si}$  or  $^{41}\text{Si}$ ) can also give important information on the evolution of the deformation near  $^{40}\text{Si}$ . We should also notice that these observables are affected by the polarization effect which is another interesting issue to be studied.

## Acknowledgment

We would like to thank E. Hiyama for valuable discussions. This work is supported by the National Natural Science Foundation of China (Grant Nos. 10905048, 10975116 and 11275160).

## References

- [1] J. Fridmann, et al., Nature (London), **435**, 922 (2005); Phys. Rev. C, **74**, 034313 (2006).
- [2] B. Bastin et al., Phys. Rev. Lett., **99**, 022503 (2007).
- [3] T. R. Werner, J. A. Sheikh, M. Misu, W. Nazarewicz, J. Rikovska, K. Heeger, A. S. Umar, and M. R. Strayer, Nucl. Phys. A, **597**, 327 (1996).
- [4] S. Peru, M. Giroda, and J. F. Berger, Eur. Phys. J. A, **9**, 35 (2000).
- [5] G. A. Lalazissis, D. Vretenar, P. Ring, M. Stoitsov, and L. M. Robledo, Phys. Rev. C, **60**, 014310 (1999).
- [6] R. Rodriguez-Guzmán, J. L. Egido, and L. M. Robledo, Phys. Rev. C, **65**, 024304 (2002).
- [7] F. Nowacki and A. Poves, Phys. Rev. C, **79**, 014310 (2009).
- [8] Z. P. Li, J. M. Yao, D. Vretenar, T. Niksic, H. Chen, and J. Meng, Phys. Rev. C, **84**, 054304 (2011).

- 
- [9] Y. Utsuno, T. Otsuka, B. A. Brown, M. Honma, T. Mizusaki, and N. Shimizu, *Phys. Rev. C*, **86**, 051301 (2012).
- [10] T. Otsuka, T. Suzuki, and Y. Utsuno, *Nucl. Phys. A*, **805**, 127 (2008).
- [11] Y. Utsuno, T. Otsuka, B. A. Brown, M. Honma, and T. Mizusaki, *AIP Conf. Proc.*, **1120**, 81 (2009).
- [12] T. Otsuka, R. Fujimoto, Y. Utsuno, B. A. Brown, M. Honma, and T. Mizusaki, *Phys. Rev. Lett.*, **87**, 082502 (2001).
- [13] T. Otsuka, T. Suzuki, R. Fujimoto, H. Grawe, and Y. Akaishi, *Phys. Rev. Lett.*, **95**, 232502 (2005).
- [14] D. Tarpanov, H. Z. Liang, N. Van Giai, and C. Stoyanov, *Phys. Rev. C*, **77**, 054316 (2008).
- [15] G. Colò, H. Sagawa, S. Fracasso, and P. F. Bortignon, *Phys. Lett. B*, **646**, 227 (2007).
- [16] D. M. Brink and F. Stancu, *Phys. Rev. C*, **75**, 064311 (2007).
- [17] T. Lesinski, M. Bender, K. Bennaceur, T. Duguet, and J. Meyer, *Phys. Rev. C*, **76**, 014312 (2007) and references therein.
- [18] C. L. Bai, H. Sagawa, H. Q. Zhang, X. Z. Zhang, G. Colò, and F. R. Xu, *Phys. Lett. B*, **675**, 28 (2009).
- [19] L. G. Cao, G. Colò, P. F. Bortignon, H. Sagawa, and L. Sciacchitano, *Phys. Rev. C*, **80**, 064304 (2009).
- [20] C. L. Bai, H. Q. Zhang, X. Z. Zhang, F. R., Xu, H. Sagawa, and G. Colò, *Phys. Rev. Lett.*, **105**, 072501 (2010).
- [21] P. Möller, J. R. Nix, W. D. Myers, and W. J. Swiatecki, *At. Data Nucl. Data Tables*, **59**, 185 (1995).
- [22] R. W. Ibbotson et al., *Phys. Rev. Lett.*, **80**, 2081 (1998).
- [23] D. Vautherin, *Phys. Rev. C*, **7**, 296 (1973).
- [24] W. Nazarewicz, T. R. Werner, and J. Dobaczewski, *Phys. Rev. C*, **50**, 2860 (1994).
- [25] S. J. Krieger, P. Bonche, H. Flocard, P. Quentin, and M. S. Weiss, *Nucl. Phys. A*, **517**, 275 (1990).
- [26] M. Bender, K. Rutz, P.-G. Reinhard, and J. A. Maruhn, *Eur. Phys. J. A*, **8**, 59 (2000).
- [27] A. Li, E. Hiyama, X. R. Zhou, and H. Sagawa, *Phys. Rev. C*, **87**, 014333 (2013).
- [28] G. Audi, A. H. Wapstra, and C. Thibault, *Nucl. Phys. A*, **729**, 337 (2003).
- [29] W. Satula, J. Dobaczewski, and W. Nazarewicz, *Phys. Rev. Lett.*, **81**, 3599 (1998).
- [30] V. Blum, G. Lauritsch, J. A. Maruhn, and P.-G. Reinhard, *J. Comput. Phys.*, **100**, 364 (1992).
- [31] H. Sagawa, X. R. Zhou, X. Z. Zhang, and T. Suzuki, *Phys. Rev. C*, **70**, 054316 (2004).
- [32] X. R. Zhou, H.-J. Schulze, H. Sagawa, C. X. Wu, and E. G. Zhao, *Phys. Rev. C*, **76**, 034312 (2007).
- [33] B. A. Brown, T. Duguet, T. Otsuka, D. Abe, and T. Suzuki, *Phys. Rev. C*, **74**, 061303 (2006).
- [34] W. Nazarewicz, *Int. Jour. Mod. Phys. E*, **2**, 51 (1993).